



Measurement of associated J/ψ - $\psi(2S)$ production cross-section in pp collisions at $\sqrt{s} = 13$ TeV

LHCb collaboration[†]

Abstract

The cross-section of associated J/ψ - $\psi(2S)$ production in proton-proton collisions at a centre-of-mass energy of $\sqrt{s} = 13$ TeV is measured using a data sample corresponding to an integrated luminosity of 4.2 fb^{-1} , collected by the LHCb experiment. The measurement is performed for both J/ψ and $\psi(2S)$ mesons having transverse momentum $p_T < 14 \text{ GeV}/c$ and rapidity $2.0 < y < 4.5$, assuming negligible polarisation of the J/ψ and $\psi(2S)$ mesons. The production cross-section is measured to be $4.5 \pm 0.7 \pm 0.3 \text{ nb}$, where the first uncertainty is statistical and the second systematic. The differential cross-sections are measured as functions of several kinematic variables of the J/ψ - $\psi(2S)$ candidates. The results are combined with a measurement of J/ψ - J/ψ production, giving a cross-section ratio between J/ψ - $\psi(2S)$ and J/ψ - J/ψ production of $0.274 \pm 0.044 \pm 0.008$, where the first uncertainty is statistical and the second systematic.

Published in JHEP 05 (2024) 259

© 2024 CERN for the benefit of the LHCb collaboration. CC BY 4.0 licence.

[†]Authors are listed at the end of this paper.

1 Introduction

Quantum chromodynamics (QCD) is the fundamental theory of the strong interaction between quarks and gluons. One of the most important properties of QCD is that the coupling constant increases with decreasing energy. A perturbative treatment can be applied at large momentum transfer, while the non-perturbative effects at small momentum transfer make theoretical calculations difficult and usually need to be described by effective theories or phenomenological models with input from experiment. The study of heavy quarkonium production in proton-proton (pp) collisions can provide important information to improve QCD calculations in the non-perturbative regime. The process involves production of a $Q\bar{Q}$ pair, where Q denotes a beauty or charm quark, followed by its hadronisation into a heavy quarkonium state. In the nonrelativistic QCD (NRQCD) approach [1–3], both colour-singlet and colour-octet states of the intermediate $Q\bar{Q}$ pair are taken into account, and the transition probabilities from the $Q\bar{Q}$ states to the heavy quarkonium are described by non-perturbative long-distance matrix elements. Although the NRQCD approach describes many aspects of quarkonium production successfully, no satisfactory solution has been achieved thus far to simultaneously describe differential cross-section and polarisation data over the whole kinematic region [4, 5]. This puzzle can be probed via the production of heavy quarkonium pairs through the single-parton scattering (SPS) process [6–9], which can provide new tests of the NRQCD approach.

Besides SPS, heavy quarkonium pairs can be produced through double-parton scattering (DPS) [10], which makes the study more complicated. The DPS process is of great relevance since it provides valuable information on the profile and correlations of partons inside the proton. A thorough understanding of DPS is crucial in some searches for physics beyond the standard model because several important sources of background, *e.g.* $Z + b\bar{b}$, $W^\pm W^\pm$, have significant DPS contributions. In DPS, the heavy quarkonium pair production is usually assumed to come from two independent partonic interactions, and the cross-section can be estimated according to [11–13]

$$\sigma_{\mathcal{Q}_1\mathcal{Q}_2}^{\text{DPS}} = \frac{1}{1 + \delta_{\mathcal{Q}_1\mathcal{Q}_2}} \frac{\sigma_{\mathcal{Q}_1}\sigma_{\mathcal{Q}_2}}{\sigma_{\text{eff}}}, \quad (1)$$

where $\delta_{\mathcal{Q}_1\mathcal{Q}_2}$ is one if the two quarkonium states \mathcal{Q}_1 and \mathcal{Q}_2 are the same and zero if they are different, $\sigma_{\mathcal{Q}_1}$ and $\sigma_{\mathcal{Q}_2}$ are the production cross-sections of single quarkonium \mathcal{Q}_1 and \mathcal{Q}_2 respectively, and σ_{eff} is an effective cross-section characterising an effective transverse overlap area between the two pairs of interacting partons.

Experimentally, it is difficult to distinguish the SPS and DPS contributions. The measurements of quarkonium pair production so far mostly separate them according to the kinematic relation between the two quarkonium decays, which is model dependent. This paper focuses on charmonium pair production. The production of J/ψ mesons associated with the χ_c state, whose charge parity is even, through SPS is forbidden at leading order in NRQCD, resulting in a large difference in the fraction of J/ψ pairs produced from feed-down of χ_c and $\psi(2S)$ mesons between SPS and DPS. The fraction of feed-down from $\psi(2S)$ production is expected to be large (around 46%) in SPS, while it is only about 20% in DPS [10]. The fraction of feed-down from χ_c production is suppressed in SPS, while it is around 50% in DPS [10]. Thus the feed-down fraction of J/ψ pairs from J/ψ - $\psi(2S)$ or J/ψ - χ_c is considered as another important test to pin down the DPS or SPS dominance.

The first evidence for J/ψ -pair production in hadron collisions was reported by the

NA3 collaboration in the 1980s [14, 15]. In recent years, the J/ψ -pair production cross-section in pp collisions was measured by the LHCb collaboration at $\sqrt{s} = 7$ TeV [16] and 13 TeV [17], by the CMS collaboration in pp collisions at $\sqrt{s} = 7$ TeV [18] and by the ATLAS collaboration at $\sqrt{s} = 8$ TeV [19]. It was also measured in $p\bar{p}$ collisions by the D0 collaboration at $\sqrt{s} = 1.96$ TeV [20]. However, the production of charmonium pairs involving other states, such as J/ψ - $\psi(2S)$ and J/ψ - χ_c has not been measured before.

In this paper, the measurement of J/ψ - $\psi(2S)$ production cross-sections in pp collisions at $\sqrt{s} = 13$ TeV is presented, using a subset of data collected by the LHCb experiment from 2016 to 2018 with specific trigger requirements, corresponding to an integrated luminosity of 4.2 fb^{-1} . The production cross-sections are measured for J/ψ and $\psi(2S)$ mesons having transverse momentum $p_T < 14 \text{ GeV}/c$ and rapidity $2.0 < y < 4.5$, assuming negligible polarisation of the J/ψ and $\psi(2S)$ mesons, since all the LHC measurements so far indicate that the polarisation of quarkonia is small [21–25]. The differential cross-sections of J/ψ - $\psi(2S)$ production as functions of several kinematic variables are also measured, as well as the cross-section ratio between J/ψ - $\psi(2S)$ and J/ψ - J/ψ production.

2 Detector and dataset

The LHCb detector [26, 27] is a single-arm forward spectrometer covering the pseudorapidity range $2 < \eta < 5$, designed for the study of particles containing b or c quarks. The detector includes a high-precision tracking system consisting of a silicon-strip vertex detector surrounding the pp interaction region, a large-area silicon-strip detector located upstream of a dipole magnet with a bending power of about 4 Tm, and three stations of silicon-strip detectors and straw drift tubes placed downstream of the magnet. The tracking system provides a measurement of the momentum, p , of charged particles with a relative uncertainty that varies from 0.5% at low momentum to 1.0% at 200 GeV/ c . The minimum distance of a track to a pp interaction point (*i.e.* primary vertex, PV), the impact parameter (IP), is measured with a resolution of $(15 + 29/p_T) \mu\text{m}$, where p_T is in GeV/ c . Different types of charged hadrons are distinguished using information from two ring-imaging Cherenkov detectors. Photons, electrons and hadrons are identified by a calorimeter system consisting of scintillating-pad and preshower detectors, an electromagnetic and a hadronic calorimeter. Muons are identified by a system composed of alternating layers of iron and multiwire proportional chambers.

The J/ψ - $\psi(2S)$ candidates are reconstructed using final states with two $\mu^+\mu^-$ pairs. The online event selection is performed by a trigger [28], which consists of a hardware stage (L0), based on information from the calorimeter and muon systems, followed by two stages of software trigger, HLT1 and HLT2, at which full event reconstruction is performed. It is required that at least one $\mu^+\mu^-$ pair fulfils the selection criteria of the L0 and HLT1 triggers. The L0 trigger selects two muons with the product of their transverse momentum $p_{T1} \times p_{T2} > 1.3^2, 1.5^2$ or $1.8^2 (\text{GeV}/c)^2$, depending on the data-taking period. The HLT1 trigger requires two good-quality tracks with $p_T > 0.3 \text{ GeV}/c$ and $p > 6 \text{ GeV}/c$, which are loosely identified as muons, to form a J/ψ or $\psi(2S)$ candidate with high invariant mass, $m_{\mu^+\mu^-} > 2.7 \text{ GeV}/c^2$ or $2.9 \text{ GeV}/c^2$, depending on the data-taking period. The HLT2 trigger requires both J/ψ and $\psi(2S)$ candidates to be reconstructed with good vertex-fit quality, and the invariant mass $m_{\mu^+\mu^-}$ is required to be within $120 \text{ MeV}/c^2$ of the known J/ψ or $\psi(2S)$ masses [29].

Simulated samples are produced to study the behaviour of signal candidates and determine the detection efficiencies. The pp collisions are modelled using PYTHIA [30, 31] with a specific LHCb configuration [32]. Decays of unstable particles are described by EVTGEN [33] with QED final-state radiation handled by PHOTOS [34]. The interactions of the generated particles with the detector are modelled using the GEANT4 toolkit [35, 36] as described in Ref. [37]. Due to limited knowledge of the associated J/ψ - $\psi(2S)$ production mechanism, the candidate selection is designed not to utilise information based on the correlation between the J/ψ and $\psi(2S)$ mesons. Therefore, the detection efficiency can be factorised into that of J/ψ and $\psi(2S)$. The efficiency factorisation is validated using a simulated sample of $\Upsilon \rightarrow J/\psi J/\psi \gamma$ decays. The J/ψ and $\psi(2S)$ efficiencies are evaluated using simulated samples of single- J/ψ and single- $\psi(2S)$ candidates. In the PYTHIA model, J/ψ and $\psi(2S)$ mesons are generated with no polarisation, and the leading order colour-singlet and colour-octet contributions [32, 38] are considered in prompt J/ψ and $\psi(2S)$ production.

3 Candidate selection

Further selections are performed offline to J/ψ - $\psi(2S)$ candidates to reduce the combinatorial background. Four muon tracks with good track-fit quality are selected and required to have $1.9 < \eta < 4.9$, $p_T > 0.65 \text{ GeV}/c$ and $p > 3 \text{ GeV}/c$, and to form two good-quality di-muon vertices. The muon identification requirement is tightened to further suppress the contribution of mis-identified tracks. The background from fake tracks is reduced by a neural-network based algorithm [39]. All events are required to have at least one reconstructed PV. For candidates with multiple PVs in the event, the one with the smallest χ_{IP}^2 is taken as the associated PV, where χ_{IP}^2 is defined as the difference in the vertex-fit χ^2 of a given PV reconstructed with and without the candidate under consideration. The four muon tracks are required to originate from the same PV. This reduces the number of pile-up candidates, *i.e.* J/ψ and $\psi(2S)$ candidates originating from two independent pp interactions, to a negligible level. A selection is performed on the pseudoproper time t_z [40] of the J/ψ and $\psi(2S)$ candidates, defined as

$$t_z = \frac{z_\psi - z_{\text{PV}}}{p_z} \times m_\psi, \quad (2)$$

where z_ψ and z_{PV} are the coordinates of the J/ψ or $\psi(2S)$ decay vertex and the PV along the beam axis z , p_z is the projection of the J/ψ or $\psi(2S)$ momentum along the z axis, and m_ψ is the known J/ψ or $\psi(2S)$ mass [29]. The t_z uncertainty σ_{t_z} is calculated by combining the uncertainties from z_ψ and z_{PV} since the uncertainty on p_z is negligible in comparison. Candidates with both J/ψ and $\psi(2S)$ mesons having $-2 < t_z < 10 \text{ ps}$ and $\sigma_{t_z} < 0.3 \text{ ps}$ are selected. After the selection, the events with multiple candidates, in particular those in which the four muons can be combined in two different ways to form a J/ψ - $\psi(2S)$ candidate, account for 1.2% of the total. According to simulation, the candidates with wrong combination of muons follow the background distribution, so their inclusion do not introduce any bias to the signal yield determination.

4 Cross-section determination

The cross-section of associated $J/\psi\text{-}\psi(2S)$ production is given by

$$\sigma_{J/\psi\text{-}\psi(2S)} = \frac{N^{\text{corr}}}{\mathcal{L} \times \mathcal{B}(J/\psi \rightarrow \mu^+\mu^-) \times \mathcal{B}(\psi(2S) \rightarrow \mu^+\mu^-)}, \quad (3)$$

where N^{corr} is the efficiency-corrected yield, \mathcal{L} is the integrated luminosity, and \mathcal{B} is the appropriate branching fraction. The integrated luminosity is $\mathcal{L} = 4.18 \pm 0.08 \text{ fb}^{-1}$ measured using the van der Meer scan method [41]. The branching fraction of the J/ψ decay is $\mathcal{B}(J/\psi \rightarrow \mu^+\mu^-) = (5.961 \pm 0.033)\%$ [29]. Under the assumption of lepton universality in electromagnetic decays, the branching fraction of the $\psi(2S)$ decay is taken to be $\mathcal{B}(\psi(2S) \rightarrow e^+e^-) = (7.93 \pm 0.17) \times 10^{-3}$ [29], taking advantage of its much smaller uncertainty compared to the muonic decay.

The $J/\psi\text{-}\psi(2S)$ signals are extracted by performing an unbinned extended maximum likelihood fit to the two-dimensional (2D) mass distribution of J/ψ and $\psi(2S)$ candidates, $(m_{\mu_1^+\mu_1^-}, m_{\mu_2^+\mu_2^-})$. The 2D mass distribution function can be factorised into the product of the two mass dimensions. Each one-dimensional mass distribution consists of the signal and combinatorial background components. The signal component is described by a sum of a double-sided Crystal Ball (DSCB) function [42] and a Gaussian function with a common mean value but different widths. All the tail parameters, the fraction of the DSCB function and the ratio between the two widths are fixed from simulation. Only the common mean value and the width of the DSCB function are left as free shape parameters. The combinatorial background distribution is modelled with an exponential function.

For $J/\psi\text{-}\psi(2S)$ candidates, there are four categories:

- a signal $J/\psi\text{-}\psi(2S)$ decay,
- a true J/ψ decay with a fake $\psi(2S)$ decay,
- a fake J/ψ decay with a true $\psi(2S)$ decay,
- and a fake J/ψ decay with a fake $\psi(2S)$ decay.

Figure 1 shows the projections of the 2D mass distribution, together with the fit result, of the $m_{\mu_1^+\mu_1^-}$ and $m_{\mu_2^+\mu_2^-}$ invariant mass combinations.

In pp collisions, J/ψ or $\psi(2S)$ mesons can be produced either directly from hard collisions of partons, through the feed-down of excited charmonium states, or via decays of beauty hadrons. The J/ψ or $\psi(2S)$ mesons from the first two sources originate from the PV and are called prompt mesons, while those from the last source originate from decay vertices of beauty hadrons, which are typically separated from the PV, and are called nonprompt mesons. The nonprompt contributions with the J/ψ or $\psi(2S)$ meson originating from b -hadron decays are subtracted by performing a maximum-likelihood fit to the 2D t_z distribution of $J/\psi\text{-}\psi(2S)$ candidates with backgrounds subtracted. The background subtraction is implemented with the *sPlot* method [43] using $m_{\mu_1^+\mu_1^-}$ and $m_{\mu_2^+\mu_2^-}$ as the discriminating variables. The t_z distribution of prompt J/ψ or $\psi(2S)$ mesons is described by the Dirac delta function $\delta(t_z)$, while that of nonprompt mesons by an exponential function. These distributions are convolved with a Gaussian detector resolution function. For a very small fraction of candidates, the true PV is not reconstructed and both J/ψ

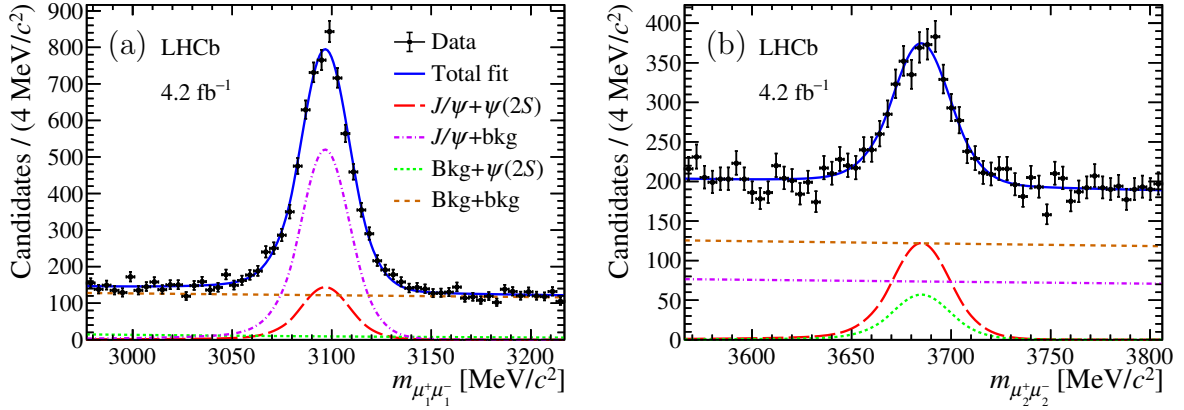


Figure 1: Distributions of (a) $m_{\mu_1^+\mu_1^-}$ and (b) $m_{\mu_2^+\mu_2^-}$ for J/ψ - $\psi(2S)$ candidates together with the projections of the fit.

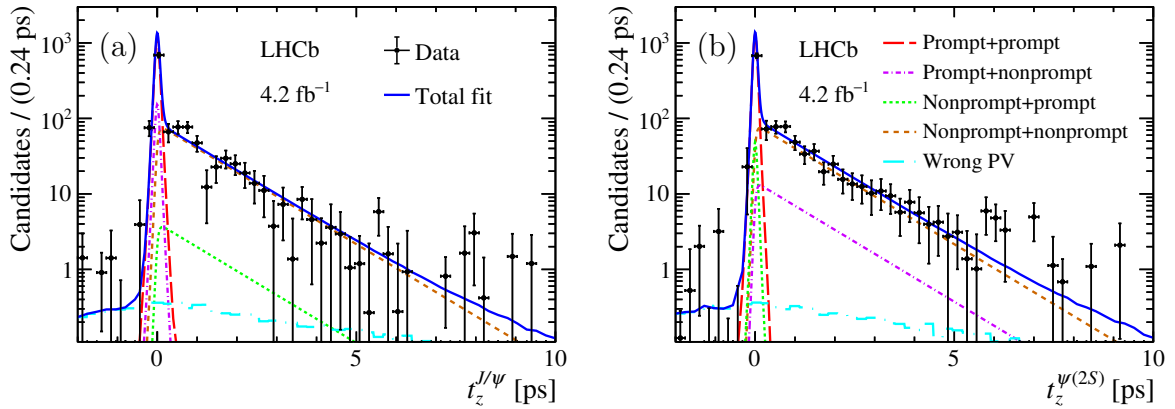


Figure 2: Distributions of (a) $t_z^{J/\psi}$ and (b) $t_z^{\psi(2S)}$ for J/ψ - $\psi(2S)$ candidates with backgrounds subtracted together with the projections of the fit.

and $\psi(2S)$ candidates are associated to the nearest reconstructed PV. The positions of the true PV and the wrongly associated PV are not correlated, which results in a broad distribution of t_z . This component can be modelled from data using event mixing, *i.e.* calculating t_z with the J/ψ or $\psi(2S)$ candidate associated to the closest PV in the next event of the sample. Figure 2 shows the projections of the 2D t_z distribution with backgrounds subtracted, together with the fit result, on $t_z^{J/\psi}$ and $t_z^{\psi(2S)}$. The yield of prompt J/ψ - $\psi(2S)$ signal candidates is 629 ± 50 .

Since the kinematics of J/ψ - $\psi(2S)$ decay are not known *a priori*, an efficiency correction is performed event-by-event as

$$N^{\text{corr}} = \sum_i \frac{w_i}{\varepsilon_i^{\text{tot}}}, \quad (4)$$

where the index i denotes each event in data, w_i is the *sWeight* [43] corresponding to the component of prompt J/ψ - $\psi(2S)$ signal candidates, and $\varepsilon_i^{\text{tot}}$ the detection efficiency. The efficiency $\varepsilon_i^{\text{tot}}$ is evaluated as the product of four components: the geometrical acceptance $\varepsilon_i^{\text{acc}}$, the efficiency of reconstruction and selection $\varepsilon_i^{\text{rec\&sel}}$, the PID efficiency $\varepsilon_i^{\text{PID}}$, and the

trigger efficiency $\varepsilon_i^{\text{trig}}$, giving

$$\varepsilon_i^{\text{tot}} = \varepsilon_i^{\text{acc}} \times \varepsilon_i^{\text{rec\&sel}} \times \varepsilon_i^{\text{PID}} \times \varepsilon_i^{\text{trig}}. \quad (5)$$

For a J/ψ - $\psi(2S)$ candidate, each efficiency factor can be parameterised as a function of the p_{T} and y of the J/ψ and $\psi(2S)$ mesons. As long as the real p_{T} and y values of both J/ψ and $\psi(2S)$ mesons are taken, it makes no difference for the efficiencies whether the candidate is produced by SPS or DPS. The possible kinematic correlation between two mesons, reflected in p_{T} and y , carries information on the production mechanism. On this basis, the efficiencies of each J/ψ - $\psi(2S)$ candidate can be factorised into those of the J/ψ and $\psi(2S)$ mesons separately, since no information related to the correlation between them is used during the reconstruction and selection process. The efficiencies $\varepsilon_i^{\text{acc}}$, $\varepsilon_i^{\text{rec\&sel}}$ and $\varepsilon_i^{\text{PID}}$ of each J/ψ - $\psi(2S)$ candidate are factorised as the product of efficiencies of the J/ψ and $\psi(2S)$ mesons as

$$\varepsilon_i(J/\psi\text{-}\psi(2S)) = \varepsilon_i(J/\psi) \times \varepsilon_i(\psi(2S)). \quad (6)$$

The trigger efficiency $\varepsilon_i^{\text{trig}}$ of each J/ψ - $\psi(2S)$ candidate is factorised as

$$\varepsilon_i^{\text{trig}}(J/\psi\text{-}\psi(2S)) = 1 - (1 - \varepsilon_i^{\text{L0\&HLT1}}(J/\psi)) (1 - \varepsilon_i^{\text{L0\&HLT1}}(\psi(2S))), \quad (7)$$

where $\varepsilon_i^{\text{L0\&HLT1}}$ is the L0-and-HLT1 trigger efficiency. The online HLT2 reconstruction algorithm is equivalent to the offline algorithm and the offline selections are tighter than the HLT2 requirements, making the HLT2 trigger fully efficient with respect to offline selected candidates. All the efficiency terms are estimated in (p_{T}, y) intervals of the J/ψ ($\psi(2S)$) meson using the simulated single- J/ψ (single- $\psi(2S)$) samples. The track reconstruction efficiency, which is part of $\varepsilon_i^{\text{rec\&sel}}$, and the PID efficiency, $\varepsilon_i^{\text{PID}}$, are calibrated using data to eliminate differences between the simulation and data [44, 45]. The efficiency-corrected signal yield is determined to be $N^{\text{corr}} = (8.9 \pm 1.4) \times 10^3$, where the statistical uncertainty is verified by the bootstrapping approach [46].

5 Systematic uncertainties

Table 1 summaries the systematic uncertainties on the cross-section measurement. Due to the small yields of the J/ψ - $\psi(2S)$ data, a larger pseudo J/ψ - $\psi(2S)$ sample is produced by combining the single- J/ψ and single- $\psi(2S)$ candidates in data randomly to reduce the statistical fluctuations in the evaluation of systematic uncertainties. The same treatment of the selection, signal extraction and the efficiency correction is applied to this pseudo sample as for the J/ψ - $\psi(2S)$ data sample.

An uncertainty is attributed to the imperfect modelling of the J/ψ ($\psi(2S)$) mass distribution. As an alternative to the sum of a DSCB function and a Gaussian function, the invariant-mass distribution of J/ψ ($\psi(2S)$) signals is described by a model derived from simulation using the kernel density estimation approach [47]. To account for the resolution difference between data and simulation, the alternative model is convolved with a Gaussian function with a mean value of zero and the width varied freely. The relative difference of the extracted signal yields using the default and alternative models is 1.7%, which is taken as the systematic uncertainty. For the measurement of differential cross-sections, this uncertainty is taken to be common to all kinematic intervals.

An uncertainty is attributed to the subtraction of nonprompt contributions. The quantity $\log(\chi_{\text{IP}}^2)$ of the J/ψ ($\psi(2S)$) meson is used for the discrimination of nonprompt components instead of the pseudoproper time t_z . The $\log(\chi_{\text{IP}}^2)$ distribution of the prompt J/ψ ($\psi(2S)$) signals is described by the sum of two Bukin functions [48] with the same peak position and asymmetry, while the nonprompt component is described by one Bukin function. The shape parameters of the Bukin functions other than the peak position and width are fixed from simulation. The relative difference of the yield of prompt J/ψ - $\psi(2S)$ signal candidates with respect to the default result, 1.9%, is taken as the systematic uncertainty. For the measurement of differential cross-sections, this uncertainty is considered common to all kinematic intervals.

A small fraction of J/ψ or $\psi(2S)$ candidates in the J/ψ - $\psi(2S)$ data may be associated to a wrong PV, which can be divided into two cases. The first is that the true PV is reconstructed but one of the J/ψ and $\psi(2S)$ candidates is associated to a wrong PV accidentally. In this case, J/ψ and $\psi(2S)$ mesons are associated to different PVs and thus are rejected by the selection. The fraction is estimated using the simulated sample of $\Upsilon \rightarrow J/\psi J/\psi \gamma$ decays to be $(0.65 \pm 0.02)\%$. The second is that the true PV is not reconstructed and both J/ψ and $\psi(2S)$ candidates are associated to the nearest reconstructed PV in this event. This is a component in the 2D t_z fit, with the fraction determined to be $(0.8 \pm 1.5)\%$. The total fraction of wrong PV events adds up to 1.5%, which is taken as a systematic uncertainty. For the measurement of differential cross-sections, the fraction is studied in several intervals of J/ψ - $\psi(2S)$ rapidities using the same method. The maximum, 2.2%, is conservatively taken as the uncertainty common to all kinematic intervals.

The limited size of the calibration samples used to determine the efficiencies can introduce a systematic uncertainty. This is studied by using pseudoexperiments, in which the efficiency in each (p_T, y) interval is sampled by Gaussian distributions with the corresponding efficiency as the mean value and the statistical uncertainty of the efficiency as the width. The width of the cross-section distribution obtained from pseudoexperiments is determined to be 0.7%, and taken as the systematic uncertainty. It varies up to 3.0% depending on the kinematic intervals for the measurement of differential cross-sections.

The binning scheme that is used to determine the efficiencies could bias the signal yield N^{corr} . For the PID efficiency, this effect is studied by varying the binning schemes of the calibration sample, and the relative difference in the cross-sections is taken as an uncertainty. For the other efficiencies, ε^{acc} , $\varepsilon^{\text{rec\&sel}}$ and $\varepsilon^{\text{trig}}$, the kernel density estimation approach [47] is used as an alternative, in which the efficiencies are determined as smoothed functions of (p_T, y) . The relative difference in the cross-sections between the default and alternative approaches is quoted as the systematic uncertainty separately for each efficiency factor. The uncertainty on the total efficiency is taken as a quadratic sum of these uncertainties on the four efficiency factors, and its value is 2.8%. For the differential cross-sections, it varies up to 5.5% depending on the kinematic intervals.

The systematic uncertainty from the track reconstruction efficiency has two sources. One is propagated from the statistical uncertainties of the correction factors due to the limited size of the calibration sample. It is evaluated to be 0.9% using pseudoexperiments. The correction factors also depend on the event multiplicity, which is not perfectly matched between the simulation and calibration samples. This introduces a systematic uncertainty of 0.8% per track, adding up to 3.2% for the J/ψ - $\psi(2S)$ signals containing four muon tracks. The track detection efficiency uncertainty is in total 3.3% with the two sources

Table 1: Summary of relative systematic uncertainties on the measurement of J/ψ - $\psi(2S)$ production cross-section. The total systematic uncertainty is the quadratic sum of the individual contributions.

Source	Uncertainty
Signal mass model	1.7%
Nonprompt contribution	1.9%
Wrong PV association	1.5%
Calibration sample statistics	0.7%
Efficiency determination	2.1%
Track reconstruction efficiency	3.3%
Trigger efficiency	0.7%
Branching fractions	2.2%
Luminosity	2.0%
Total	5.9%

added in quadrature. For the differential cross-sections, the first term varies up to 4.2%, while the second is considered to be common to all kinematic intervals.

The systematic uncertainty associated with the trigger efficiency is evaluated by comparing the efficiency determined from the simulated single- J/ψ sample to that from the single- J/ψ data. The trigger efficiency is determined using a subset of events that fulfil the trigger requirement with the J/ψ signals excluded [49]. Due to the small yields of the $\psi(2S)$ sample, the ratio of trigger efficiencies between data and simulation determined using the J/ψ events is also applied to $\psi(2S)$ mesons. The relative difference in the J/ψ - $\psi(2S)$ cross-section between using the trigger efficiency obtained from data and simulation is 0.7%, and is taken as a systematic uncertainty. For the differential cross-sections, the quoted uncertainty varies up to 7.5% depending on the kinematic intervals.

The uncertainties on the branching fractions lead to an uncertainty of 2.2% on the measured cross-section. The luminosity is determined with a relative uncertainty of 2.0% using the methods described in Ref. [41]. With these uncertainties due to independent effects added in quadrature, the total systematic uncertainty on the J/ψ - $\psi(2S)$ production cross-section is determined to be 5.9%.

6 Production cross-section and cross-section ratio

The cross-section of associated J/ψ - $\psi(2S)$ production with both J/ψ and $\psi(2S)$ mesons having $p_T < 14$ GeV/ c and $2.0 < y < 4.5$ is measured to be

$$\sigma_{J/\psi-\psi(2S)} = 4.5 \pm 0.7 \text{ (stat)} \pm 0.3 \text{ (syst) nb,}$$

under the assumption of negligible polarisation of the J/ψ and $\psi(2S)$ mesons. The detection efficiency of J/ψ and $\psi(2S)$ mesons depends on their polarisation, especially on the polarisation parameter λ_θ [24, 25, 50, 51]. If the polarisation parameter λ_θ is assumed to be +0.2 (−0.2) for both J/ψ and $\psi(2S)$ mesons in the helicity frame, the cross-section of J/ψ - $\psi(2S)$ production changes by +6.5% (−6.6%).

According to Eq. 1, the ratio between the product of single- J/ψ and single- $\psi(2S)$

cross-sections and the $J/\psi\text{-}\psi(2S)$ cross-section, $\frac{\sigma_{J/\psi}\sigma_{\psi(2S)}}{\sigma_{J/\psi\text{-}\psi(2S)}}$ is a lower limit of σ_{eff} . It can be interpreted as the effective cross-section σ_{eff} if the $J/\psi\text{-}\psi(2S)$ candidates are produced entirely from the DPS process. The cross-section ratio is determined to be

$$\frac{\sigma_{J/\psi}\sigma_{\psi(2S)}}{\sigma_{J/\psi\text{-}\psi(2S)}} = 7.1 \pm 1.1 \text{ (stat)} \pm 0.8 \text{ (syst)} \text{ mb},$$

where the single- J/ψ cross-section in pp collisions at $\sqrt{s} = 13 \text{ TeV}$ with $p_{\text{T}} < 14 \text{ GeV}/c$ and $2.0 < y < 4.5$ is $\sigma_{J/\psi} = 15.03 \pm 0.94 \text{ }\mu\text{b}$ [50]. The production cross-section of $\psi(2S)$ mesons in the range of $2 < p_{\text{T}} < 14 \text{ GeV}/c$ and $2.0 < y < 4.5$ in pp collisions at $\sqrt{s} = 13 \text{ TeV}$ is measured to be $1.42 \pm 0.10 \text{ }\mu\text{b}$ by LHCb [51]. The $\psi(2S)$ cross-section with $p_{\text{T}} < 2 \text{ GeV}/c$ and $2.0 < y < 4.5$ is estimated to be $0.70 \pm 0.11 \text{ }\mu\text{b}$ [50, 52] assuming that the production ratio of J/ψ and $\psi(2S)$ does not depend on the collision energy [53]. Combining these, the single- $\psi(2S)$ cross-section in the fiducial range $p_{\text{T}} < 14 \text{ GeV}/c$ and $2.0 < y < 4.5$ is estimated to be $\sigma_{\psi(2S)} = 2.12 \pm 0.15 \text{ }\mu\text{b}$. The systematic uncertainties of the single- J/ψ , single- $\psi(2S)$ and $J/\psi\text{-}\psi(2S)$ cross-sections are treated as uncorrelated.

6.1 Differential cross-sections

The differential cross-section of $J/\psi\text{-}\psi(2S)$ production is measured as a function of the absolute value of the rapidity difference between the J/ψ and $\psi(2S)$ mesons Δy , the absolute value of the difference in the azimuthal angle ϕ between the J/ψ and $\psi(2S)$ mesons $\Delta\phi$, the transverse momentum $p_{\text{T}}^{J/\psi\text{-}\psi(2S)}$, rapidity $y_{J/\psi\text{-}\psi(2S)}$ and invariant mass $m_{J/\psi\text{-}\psi(2S)}$ of the $J/\psi\text{-}\psi(2S)$ candidates. The binning scheme is chosen to have adequate and approximately equal signal yields in each bin. Due to the limited signal yields, the differential cross-sections of $J/\psi\text{-}\psi(2S)$ production are calculated using the *sWeights* based on the global mass fit and global t_z fit rather than from the fit in each kinematic interval. The potential correlation between these kinematic variables and the discriminating variables used in the *sPlot* method may bias the signal yields. Correction factors are thus obtained using a pseudo $J/\psi\text{-}\psi(2S)$ sample produced by combining single- J/ψ and single- $\psi(2S)$ candidates in data randomly. They are calculated as the ratio of yields obtained from the fit in each kinematic interval and from the global *sWeights*. The uncertainties on the correction factors come from the limited size of the pseudosample, resulting in another systematic uncertainty on the differential cross-sections of $J/\psi\text{-}\psi(2S)$ production. It varies up to 10.7% depending on the kinematic intervals. The other systematic uncertainties on differential cross-sections are presented in Section 5. The measured differential cross-sections of $J/\psi\text{-}\psi(2S)$ production are shown in Figure 3, and listed in Tables 2–6 in Appendix A.

In the NRQCD approach, explicit calculations [7] indicate the colour-octet contributions are much smaller than colour-singlet contributions. The incomplete (not including loop diagrams) next-to-leading order colour-singlet (NLO* CS) predictions [54] of $J/\psi\text{-}\psi(2S)$ production in the SPS process can be obtained from HELAC-Onia [55, 56], an automatic matrix element generator for heavy quarkonium physics. The NLO* CS predictions are compared with the measured $J/\psi\text{-}\psi(2S)$ production cross-sections as shown in Figure 3. The theoretical uncertainties include the uncertainty due to factorisation and renormalisation scales, which is dominant, and the PDF uncertainty. The data and theory

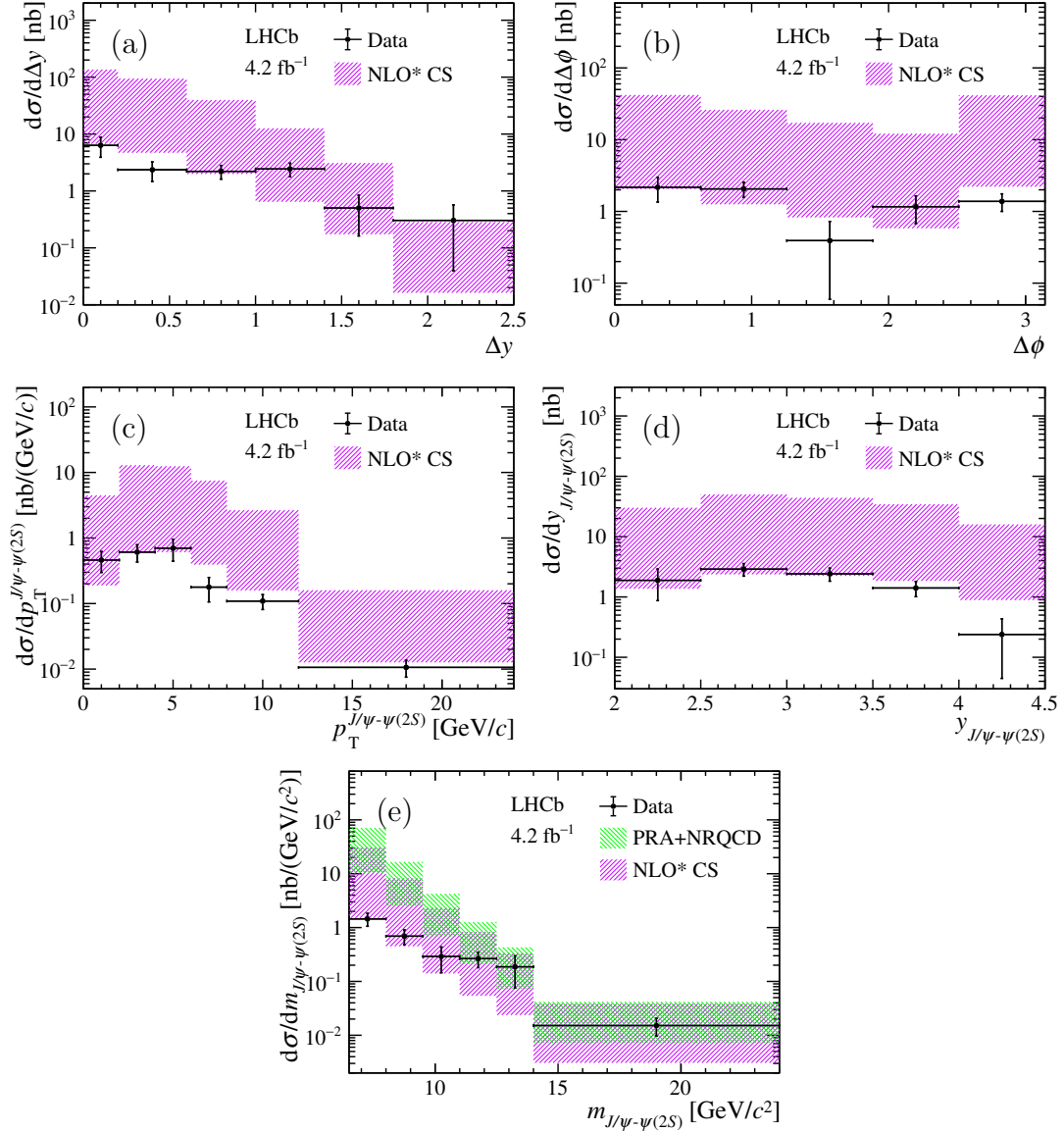


Figure 3: Differential cross-section of $J/\psi\text{-}\psi(2S)$ production as a function of (a) Δy , (b) $\Delta\phi$, (c) $p_{\text{T}}^{J/\psi\text{-}\psi(2S)}$, (d) $y_{J/\psi\text{-}\psi(2S)}$ and (e) $m_{J/\psi\text{-}\psi(2S)}$, compared with the NLO* CS predictions for SPS [54–56]. The $m_{J/\psi\text{-}\psi(2S)}$ spectrum is also compared with the PRA+NRQCD predictions for SPS [57]. The data contain contributions from both SPS and DPS.

are consistent within the large theoretical uncertainties, albeit the DPS contribution is not subtracted from the measurements.

As shown in Figure 3(e), the $m_{J/\psi\text{-}\psi(2S)}$ spectrum is also compared with the SPS predictions combining the parton Reggeization approach (PRA) [58] and the NRQCD factorisation approach [57], which includes a subset of higher-order QCD corrections in an infrared-safe way without ad-hoc kinematic cuts. Only the scale uncertainties are considered in the predictions. The PRA+NRQCD predictions for SPS are larger than the SPS+DPS data at small $m_{J/\psi\text{-}\psi(2S)}$, and consistent with them at large $m_{J/\psi\text{-}\psi(2S)}$.

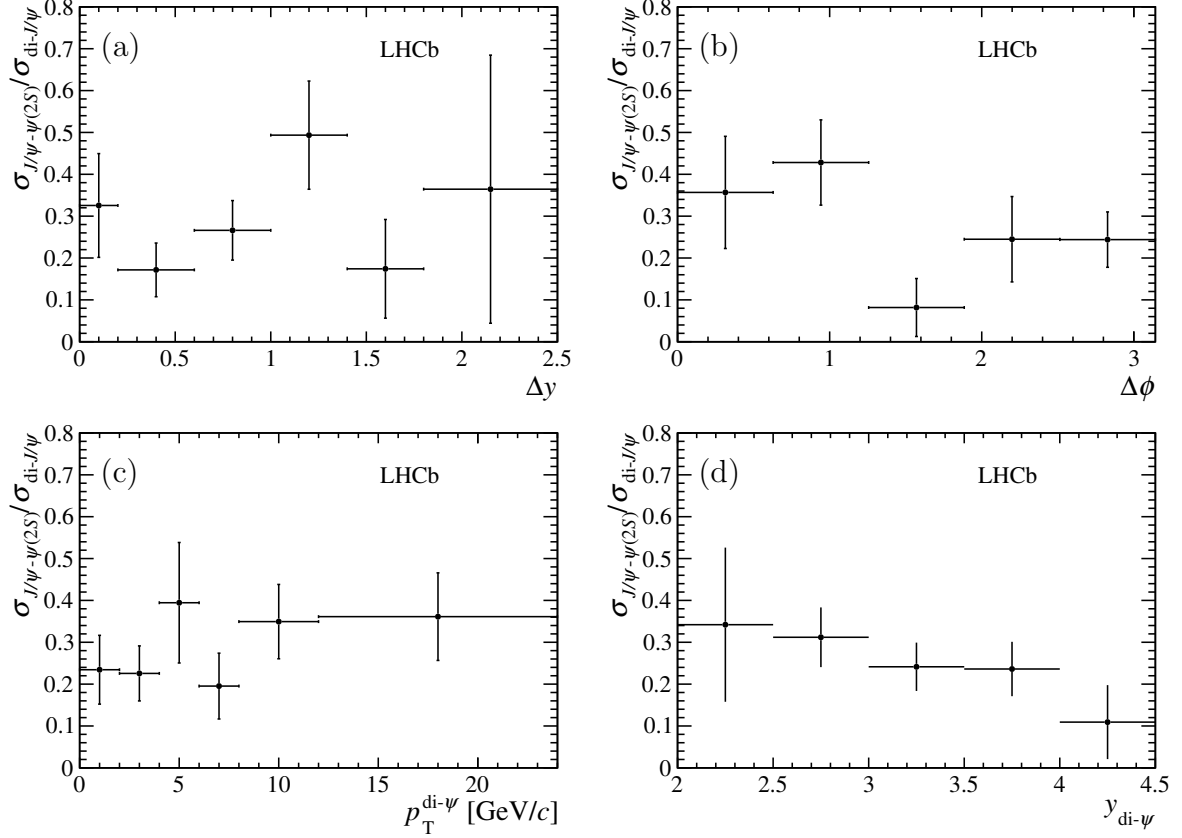


Figure 4: Cross-section ratios between J/ψ - $\psi(2S)$ and J/ψ - J/ψ production as a function of (a) Δy , (b) $\Delta\phi$, (c) $p_T^{\text{di-}\psi}$ and (d) $y_{\text{di-}\psi}$. The error bars represent the statistical and systematic uncertainties added in quadrature. The symbol di- ψ indicates J/ψ - J/ψ or J/ψ - $\psi(2S)$.

6.2 Cross-section ratio between J/ψ - $\psi(2S)$ and J/ψ - J/ψ production

The cross-section ratio between J/ψ - $\psi(2S)$ and J/ψ - J/ψ production is measured to be

$$\frac{\sigma_{J/\psi-\psi(2S)}}{\sigma_{J/\psi-J/\psi}} = 0.274 \pm 0.044 \text{ (stat)} \pm 0.008 \text{ (syst)},$$

in which the J/ψ - J/ψ production measurement is performed under a similar strategy as this analysis, as described in Ref. [59]. The systematic uncertainties due to the signal mass model, nonprompt contribution, wrong PV association, efficiency determination, multiplicity dependence of the track detection efficiency, trigger efficiency and luminosity measurement are thus assumed to be fully correlated. The uncertainties from the branching fractions cancel partially and the remaining uncertainty is 2.2% on the cross-section ratio. The uncertainties due to calibration sample sizes are considered uncorrelated. The statistical uncertainty on the cross-section ratio is dominant. The ratio is predicted to be 0.94 ± 0.30 for SPS [10], and 0.282 ± 0.027 for DPS, according to Eq. 1 and the measured single- J/ψ and single- $\psi(2S)$ cross-sections [50–52] assuming that the σ_{eff} is the same for these two processes. The measured value is much smaller than the SPS prediction and consistent with the DPS prediction, indicating a prominent DPS contribution to charmonium pair production.

The cross-section ratio is also measured as a function of Δy , $\Delta\phi$, $p_{\text{T}}^{\text{di-}\psi}$ and $y_{\text{di-}\psi}$, as shown in Figure 4. The symbol di- ψ indicates J/ψ - J/ψ or J/ψ - $\psi(2S)$. The results are also presented in Tables 7–10 in Appendix A. No clear dependence of the cross-section ratio on the kinematic variables is seen given the large uncertainties so far.

7 Conclusion

The cross-section of associated J/ψ - $\psi(2S)$ production in pp collisions at $\sqrt{s} = 13$ TeV is measured to be 4.5 ± 0.7 (stat) ± 0.3 (syst) nb for J/ψ and $\psi(2S)$ mesons with $p_{\text{T}} < 14$ GeV/ c and $2.0 < y < 4.5$, using a data sample corresponding to an integrated luminosity of 4.2 fb^{-1} collected by the LHCb experiment. The differential cross-sections of J/ψ - $\psi(2S)$ production are measured as functions of Δy , $\Delta\phi$, $p_{\text{T}}^{J/\psi-\psi(2S)}$, $y_{J/\psi-\psi(2S)}$ and $m_{J/\psi-\psi(2S)}$, and compared to the NLO* CS predictions for the SPS process. The obtained results are consistent with the theory given the presence of large theoretical uncertainties, although the DPS contribution is not subtracted from the measurement. The PRA+NRQCD predictions for SPS are larger than the data at small $m_{J/\psi-\psi(2S)}$ and consistent with them at large $m_{J/\psi-\psi(2S)}$. The cross-section ratio between J/ψ - $\psi(2S)$ and J/ψ - J/ψ production is also measured, and found to be significantly smaller than the SPS prediction and consistent with the DPS expectation. Previously [17–20], a prominent DPS contribution to the charmonium pair production was established mainly from the study of the kinematic relation of the two charmonia states. This is confirmed in this paper in a novel way.

Acknowledgements

We would like to thank H.-S. Shao, J.-P. Lansberg, Z.-G. He and M. A. Nefedov for the helpful inputs on theoretical calculations of the J/ψ - $\psi(2S)$ production. We express our gratitude to our colleagues in the CERN accelerator departments for the excellent performance of the LHC. We thank the technical and administrative staff at the LHCb institutes. We acknowledge support from CERN and from the national agencies: CAPES, CNPq, FAPERJ and FINEP (Brazil); MOST and NSFC (China); CNRS/IN2P3 (France); BMBF, DFG and MPG (Germany); INFN (Italy); NWO (Netherlands); MNiSW and NCN (Poland); MCID/IFA (Romania); MICINN (Spain); SNSF and SER (Switzerland); NASU (Ukraine); STFC (United Kingdom); DOE NP and NSF (USA). We acknowledge the computing resources that are provided by CERN, IN2P3 (France), KIT and DESY (Germany), INFN (Italy), SURF (Netherlands), PIC (Spain), GridPP (United Kingdom), CSCS (Switzerland), IFIN-HH (Romania), CBPF (Brazil), and Polish WLCG (Poland). We are indebted to the communities behind the multiple open-source software packages on which we depend. Individual groups or members have received support from ARC and ARDC (Australia); Key Research Program of Frontier Sciences of CAS, CAS PIFI, CAS CCEPP, Fundamental Research Funds for the Central Universities, and Sci. & Tech. Program of Guangzhou (China); Minciencias (Colombia); EPLANET, Marie Skłodowska-Curie Actions, ERC and NextGenerationEU (European Union); A*MIDEX, ANR, IPhU and Labex P2IO, and Région Auvergne-Rhône-Alpes (France); AvH Foundation (Germany); ICSC (Italy); GVA, XuntaGal, GENCAT, Inditex, InTalent and Prog. Atracción Talento, CM (Spain); SRC (Sweden); the Leverhulme Trust, the Royal Society and UKRI (United Kingdom).

A Differential cross-sections and cross-section ratios

The measured differential cross-sections of $J/\psi\text{-}\psi(2S)$ production as functions of Δy , $\Delta\phi$, $p_{\text{T}}^{J/\psi\text{-}\psi(2S)}$, $y_{J/\psi\text{-}\psi(2S)}$ and $m_{J/\psi\text{-}\psi(2S)}$ are listed in Tables 2–6. The cross-section ratios between $J/\psi\text{-}\psi(2S)$ and $J/\psi\text{-}J/\psi$ production as functions of Δy , $\Delta\phi$, $p_{\text{T}}^{\text{di-}\psi}$ and $y_{\text{di-}\psi}$ are listed in Tables 7–10.

Table 2: Differential cross-section $d\sigma/d\Delta y$ [nb] of $J/\psi\text{-}\psi(2S)$ production. The first uncertainty is statistical and the second systematic.

Δy	$d\sigma/d\Delta y$ [nb]
0.0–0.2	$6.33 \pm 2.37 \pm 0.55$
0.2–0.6	$2.36 \pm 0.87 \pm 0.15$
0.6–1.0	$2.21 \pm 0.58 \pm 0.15$
1.0–1.4	$2.44 \pm 0.62 \pm 0.19$
1.4–1.8	$0.50 \pm 0.34 \pm 0.05$
1.8–2.5	$0.30 \pm 0.26 \pm 0.04$

Table 3: Differential cross-section $d\sigma/d\Delta\phi$ [nb] of $J/\psi\text{-}\psi(2S)$ production. The first uncertainty is statistical and the second systematic.

$\Delta\phi/\pi$	$d\sigma/d\Delta\phi$ [nb]
0.0–0.2	$16.31 \pm 0.80 \pm 1.22$
0.2–0.4	$15.47 \pm 0.47 \pm 1.12$
0.4–0.6	$2.94 \pm 0.33 \pm 0.24$
0.6–0.8	$8.73 \pm 0.48 \pm 0.64$
0.8–1.0	$10.36 \pm 0.36 \pm 0.76$

Table 4: Differential cross-section $d\sigma/dp_{\text{T}}^{J/\psi\text{-}\psi(2S)}$ [nb/(GeV/c)] of $J/\psi\text{-}\psi(2S)$ production. The first uncertainty is statistical and the second systematic.

$p_{\text{T}}^{J/\psi\text{-}\psi(2S)}$ [GeV/c]	$d\sigma/dp_{\text{T}}^{J/\psi\text{-}\psi(2S)}$ [nb/(GeV/c)]
0–2	$0.461 \pm 0.158 \pm 0.039$
2–4	$0.609 \pm 0.174 \pm 0.045$
4–6	$0.699 \pm 0.252 \pm 0.049$
6–8	$0.178 \pm 0.071 \pm 0.013$
8–12	$0.109 \pm 0.027 \pm 0.008$
12–24	$0.011 \pm 0.003 \pm 0.001$

Table 5: Differential cross-section $d\sigma/dy_{J/\psi-\psi(2S)}$ [nb] of $J/\psi-\psi(2S)$ production. The first uncertainty is statistical and the second systematic.

$y_{J/\psi-\psi(2S)}$	$d\sigma/dy_{J/\psi-\psi(2S)}$ [nb]
2.0–2.5	$1.89 \pm 0.99 \pm 0.22$
2.5–3.0	$2.89 \pm 0.64 \pm 0.21$
3.0–3.5	$2.42 \pm 0.57 \pm 0.16$
3.5–4.0	$1.41 \pm 0.38 \pm 0.12$
4.0–4.5	$0.24 \pm 0.19 \pm 0.04$

Table 6: Differential cross-section $d\sigma/dm_{J/\psi-\psi(2S)}$ [nb/(GeV/c²)] of $J/\psi-\psi(2S)$ production. The first uncertainty is statistical and the second systematic.

$m_{J/\psi-\psi(2S)}$ [GeV/c ²]	$d\sigma/dm_{J/\psi-\psi(2S)}$ [nb/(GeV/c ²)]
6.5–8.0	$1.446 \pm 0.378 \pm 0.101$
8.0–9.5	$0.693 \pm 0.207 \pm 0.047$
9.5–11.0	$0.291 \pm 0.144 \pm 0.023$
11.0–12.5	$0.265 \pm 0.082 \pm 0.022$
12.5–14.0	$0.187 \pm 0.110 \pm 0.019$
14.0–24.0	$0.015 \pm 0.005 \pm 0.001$

Table 7: Cross-section ratio between $J/\psi-\psi(2S)$ and di- J/ψ production $\sigma_{J/\psi-\psi(2S)}/\sigma_{\text{di-}J/\psi}$ in intervals of Δy . The first uncertainty is statistical and the second systematic.

Δy	$\sigma_{J/\psi-\psi(2S)}/\sigma_{\text{di-}J/\psi}$
0.0–2.2	$0.33 \pm 0.12 \pm 0.02$
0.2–0.6	$0.17 \pm 0.06 \pm 0.01$
0.6–1.0	$0.27 \pm 0.07 \pm 0.01$
1.0–1.4	$0.49 \pm 0.13 \pm 0.03$
1.4–1.8	$0.17 \pm 0.12 \pm 0.01$
1.8–2.5	$0.36 \pm 0.32 \pm 0.05$

Table 8: Cross-section ratio between $J/\psi-\psi(2S)$ and di- J/ψ production $\sigma_{J/\psi-\psi(2S)}/\sigma_{\text{di-}J/\psi}$ in intervals of $\Delta\phi$. The first uncertainty is statistical and the second systematic.

$\Delta\phi/\pi$	$\sigma_{J/\psi-\psi(2S)}/\sigma_{\text{di-}J/\psi}$
0–2	$0.36 \pm 0.13 \pm 0.02$
2–4	$0.43 \pm 0.10 \pm 0.02$
4–6	$0.08 \pm 0.07 \pm 0.00$
6–8	$0.24 \pm 0.10 \pm 0.01$
8–12	$0.24 \pm 0.06 \pm 0.01$

Table 9: Cross-section ratio between $J/\psi\text{-}\psi(2S)$ and $\text{di-}J/\psi$ $\sigma_{J/\psi\text{-}\psi(2S)}/\sigma_{\text{di-}J/\psi}$ in intervals of $p_{\text{T}}^{\text{di-}\psi}$ [GeV/ c]. The first uncertainty is statistical and the second systematic.

$p_{\text{T}}^{\text{di-}\psi}$ [GeV/ c]	$\sigma_{J/\psi\text{-}\psi(2S)}/\sigma_{\text{di-}J/\psi}$
0–2	$0.23 \pm 0.08 \pm 0.01$
2–4	$0.23 \pm 0.06 \pm 0.01$
4–6	$0.39 \pm 0.14 \pm 0.02$
6–8	$0.20 \pm 0.08 \pm 0.01$
8–12	$0.35 \pm 0.09 \pm 0.02$
12–24	$0.36 \pm 0.10 \pm 0.03$

Table 10: Cross-section ratio between $J/\psi\text{-}\psi(2S)$ and $\text{di-}J/\psi$ $\sigma_{J/\psi\text{-}\psi(2S)}/\sigma_{\text{di-}J/\psi}$ in intervals of $y_{\text{di-}\psi}$. The first uncertainty is statistical and the second systematic.

$y_{\text{di-}\psi}$	$\sigma_{J/\psi\text{-}\psi(2S)}/\sigma_{\text{di-}J/\psi}$
2.0–2.5	$0.34 \pm 0.18 \pm 0.03$
2.5–3.0	$0.31 \pm 0.07 \pm 0.01$
3.0–3.5	$0.24 \pm 0.06 \pm 0.01$
3.5–4.0	$0.24 \pm 0.06 \pm 0.01$
4.0–4.5	$0.11 \pm 0.09 \pm 0.01$

References

- [1] G. T. Bodwin, E. Braaten, and G. P. Lepage, *Rigorous QCD analysis of inclusive annihilation and production of heavy quarkonium*, Phys. Rev. **D51** (1995) 1125, arXiv:hep-ph/9407339.
- [2] P. L. Cho and A. K. Leibovich, *Color octet quarkonia production*, Phys. Rev. **D53** (1996) 150, arXiv:hep-ph/9505329.
- [3] P. L. Cho and A. K. Leibovich, *Color octet quarkonia production. 2.*, Phys. Rev. **D53** (1996) 6203, arXiv:hep-ph/9511315.
- [4] H. S. Shao *et al.*, *Yields and polarizations of prompt J/ψ and $\psi(2S)$ production in hadronic collisions*, JHEP **05** (2015) 103, arXiv:1411.3300.
- [5] P. Zhang, C. Meng, Y.-Q. Ma, and K.-T. Chao, *Gluon fragmentation into $^3P_J^{[1,8]}$ quark pair and test of NRQCD factorization at two-loop level*, JHEP **08** (2021) 111, arXiv:2011.04905.
- [6] L.-P. Sun, H. Han, and K.-T. Chao, *Impact of J/ψ pair production at the LHC and predictions in nonrelativistic QCD*, Phys. Rev. **D94** (2016) 074033, arXiv:1404.4042.
- [7] J.-P. Lansberg, H.-S. Shao, N. Yamanaka, and Y.-J. Zhang, *Prompt J/ψ -pair production at the LHC: impact of loop-induced contributions and of the colour-octet mechanism*, Eur. Phys. J. **C79** (2019) 1006, arXiv:1906.10049.
- [8] A. K. Likhoded, A. V. Luchinsky, and S. V. Poslavsky, *Production of $J/\psi + \chi_c$ and $J/\psi + J/\psi$ with real gluon emission at LHC*, Phys. Rev. **D94** (2016) 054017, arXiv:1606.06767.
- [9] S. P. Baranov, *Pair production of J/ψ mesons in the k_t -factorization approach*, Phys. Rev. **D84** (2011) 054012.
- [10] J.-P. Lansberg and H.-S. Shao, *J/ψ -pair production at large momenta: Indications for double parton scatterings and large α_s^5 contributions*, Phys. Lett. **B751** (2015) 479, arXiv:1410.8822.
- [11] G. Calucci and D. Treleani, *Mini-jets and the two-body parton correlation*, Phys. Rev. **D57** (1998) 503, arXiv:hep-ph/9707389.
- [12] G. Calucci and D. Treleani, *Proton structure in transverse space and the effective cross-section*, Phys. Rev. **D60** (1999) 054023, arXiv:hep-ph/9902479.
- [13] A. Del Fabbro and D. Treleani, *Scale factor in double parton collisions and parton densities in transverse space*, Phys. Rev. **D63** (2001) 057901, arXiv:hep-ph/0005273.
- [14] NA3 collaboration, J. Badier *et al.*, *Evidence for $\psi\psi$ production in π^- interactions at 150- GeV/c and 280- GeV/c*, Phys. Lett. **B114** (1982) 457.
- [15] NA3 collaboration, J. Badier *et al.*, *$\psi\psi$ production and limits on beauty meson production from 400- GeV/c protons*, Phys. Lett. **B158** (1985) 85.





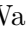


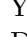
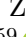

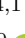
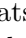










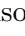
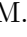


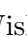



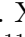
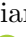
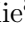

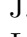

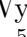




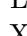

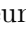
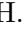

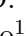
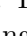

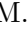







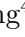




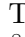
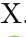
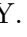
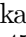


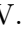
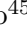
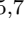
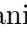
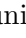




- [16] LHCb collaboration, R. Aaij *et al.*, *Observation of J/ψ -pair production in pp collisions at $\sqrt{s} = 7$ TeV*, Phys. Lett. **B707** (2012) 52, arXiv:1109.0963.
- [17] LHCb collaboration, R. Aaij *et al.*, *Measurement of the J/ψ pair production cross-section in pp collisions at $\sqrt{s} = 13$ TeV*, JHEP **06** (2017) 047, Erratum *ibid.* **10** (2017) 068, arXiv:1612.07451.
- [18] CMS collaboration, V. Khachatryan *et al.*, *Measurement of prompt J/ψ pair production in pp collisions at $\sqrt{s} = 7$ TeV*, JHEP **09** (2014) 094, arXiv:1406.0484.
- [19] ATLAS collaboration, M. Aaboud *et al.*, *Measurement of the prompt J/ψ pair production cross-section in pp collisions at $\sqrt{s} = 8$ TeV with the ATLAS detector*, Eur. Phys. J. **C77** (2017) 76, arXiv:1612.02950.
- [20] D0 collaboration, V. M. Abazov *et al.*, *Observation and studies of double J/ψ production at the Tevatron*, Phys. Rev. **D90** (2014) 111101, arXiv:1406.2380.
- [21] ALICE collaboration, B. Abelev *et al.*, *J/ψ polarization in pp collisions at $\sqrt{s} = 7$ TeV*, Phys. Rev. Lett. **108** (2012) 082001, arXiv:1111.1630.
- [22] CMS collaboration, S. Chatrchyan *et al.*, *Measurement of the prompt J/ψ and $\psi(2S)$ polarizations in pp collisions at $\sqrt{s} = 7$ TeV*, Phys. Lett. **B727** (2013) 381, arXiv:1307.6070.
- [23] CMS collaboration, S. Chatrchyan *et al.*, *Measurement of the $\Upsilon(1S)$, $\Upsilon(2S)$ and $\Upsilon(3S)$ polarizations in pp collisions at $\sqrt{s} = 7$ TeV*, Phys. Rev. Lett. **110** (2013) 081802, arXiv:1209.2922.
- [24] LHCb collaboration, R. Aaij *et al.*, *Measurement of J/ψ polarization in pp collisions at $\sqrt{s} = 7$ TeV*, Eur. Phys. J. **C73** (2013) 2631, arXiv:1307.6379.
- [25] LHCb collaboration, R. Aaij *et al.*, *Measurement of $\psi(2S)$ polarisation in pp collisions at $\sqrt{s} = 7$ TeV*, Eur. Phys. J. **C74** (2014) 2872, arXiv:1403.1339.
- [26] LHCb collaboration, A. A. Alves Jr. *et al.*, *The LHCb detector at the LHC*, JINST **3** (2008) S08005.
- [27] LHCb collaboration, R. Aaij *et al.*, *LHCb detector performance*, Int. J. Mod. Phys. **A30** (2015) 1530022, arXiv:1412.6352.
- [28] R. Aaij *et al.*, *The LHCb trigger and its performance in 2011*, JINST **8** (2013) P04022, arXiv:1211.3055.
- [29] Particle Data Group, R. L. Workman *et al.*, *Review of particle physics*, PTEP **2022** (2022) 083C01.
- [30] T. Sjöstrand, S. Mrenna, and P. Skands, *A brief introduction to PYTHIA 8.1*, Comput. Phys. Commun. **178** (2008) 852, arXiv:0710.3820.
- [31] T. Sjöstrand, S. Mrenna, and P. Skands, *PYTHIA 6.4 physics and manual*, JHEP **05** (2006) 026, arXiv:hep-ph/0603175.

- [32] I. Belyaev *et al.*, *Handling of the generation of primary events in Gauss, the LHCb simulation framework*, J. Phys. Conf. Ser. **331** (2011) 032047.
- [33] D. J. Lange, *The EvtGen particle decay simulation package*, Nucl. Instrum. Meth. **A462** (2001) 152.
- [34] N. Davidson, T. Przedzinski, and Z. Was, *PHOTOS interface in C++: Technical and physics documentation*, Comp. Phys. Comm. **199** (2016) 86, [arXiv:1011.0937](#).
- [35] Geant4 collaboration, J. Allison *et al.*, *Geant4 developments and applications*, IEEE Trans. Nucl. Sci. **53** (2006) 270.
- [36] Geant4 collaboration, S. Agostinelli *et al.*, *Geant4—A simulation toolkit*, Nucl. Instrum. Meth. **A506** (2003) 250.
- [37] M. Clemencic *et al.*, *The LHCb simulation application, Gauss: Design, evolution and experience*, J. Phys. Conf. Ser. **331** (2011) 032023.
- [38] M. Bargiotti and V. Vagnoni, *Heavy quarkonia sector in PYTHIA 6.324: Tuning, validation and perspectives at LHC(b)*, CERN-LHCB-2007-042, 2007.
- [39] M. De Cian, S. Farry, P. Seyfert, and S. Stahl, *Fast neural-net based fake track rejection in the LHCb reconstruction*, LHCb-PUB-2017-011, 2017.
- [40] LHCb collaboration, R. Aaij *et al.*, *Measurement of J/ψ production in pp collisions at $\sqrt{s} = 7\text{ TeV}$* , Eur. Phys. J. **C71** (2011) 1645, [arXiv:1103.0423](#).
- [41] LHCb collaboration, R. Aaij *et al.*, *Precision luminosity measurements at LHCb*, JINST **9** (2014) P12005, [arXiv:1410.0149](#).
- [42] T. Skwarnicki, *A study of the radiative cascade transitions between the Upsilon-prime and Upsilon resonances*, PhD thesis, Institute of Nuclear Physics, Krakow, 1986, DESY-F31-86-02.
- [43] M. Pivk and F. R. Le Diberder, *sPlot: A statistical tool to unfold data distributions*, Nucl. Instrum. Meth. **A555** (2005) 356, [arXiv:physics/0402083](#).
- [44] LHCb collaboration, R. Aaij *et al.*, *Measurement of the track reconstruction efficiency at LHCb*, JINST **10** (2015) P02007, [arXiv:1408.1251](#).
- [45] F. Archilli *et al.*, *Performance of the muon identification at LHCb*, JINST **8** (2013) P10020, [arXiv:1306.0249](#).
- [46] B. Efron, *Bootstrap methods: Another look at the jackknife*, Annals Statist. **7** (1979) 1.
- [47] K. S. Cranmer, *Kernel estimation in high-energy physics*, Comput. Phys. Commun. **136** (2001) 198, [arXiv:hep-ex/0011057](#).
- [48] A. D. Bukin, *Fitting function for asymmetric peaks*, [arXiv:0711.4449](#).
- [49] S. Tolk, J. Albrecht, F. Dettori, and A. Pellegrino, *Data driven trigger efficiency determination at LHCb*, LHCb-PUB-2014-039, 2014.

- [50] LHCb collaboration, R. Aaij *et al.*, *Measurement of forward J/ψ production cross-sections in pp collisions at $\sqrt{s} = 13$ TeV*, JHEP **10** (2015) 172, Erratum *ibid.* **05** (2017) 063, [arXiv:1509.00771](#).
- [51] LHCb collaboration, R. Aaij *et al.*, *Measurement of $\psi(2S)$ production cross-sections in proton-proton collisions at $\sqrt{s} = 7$ and 13 TeV*, Eur. Phys. J. **C80** (2020) 185, [arXiv:1908.03099](#).
- [52] LHCb collaboration, R. Aaij *et al.*, *Measurement of $\psi(2S)$ meson production in pp collisions at $\sqrt{s} = 7$ TeV*, Eur. Phys. J. **C72** (2012) 2100, Erratum *ibid.* **C80** (2020) 49, [arXiv:1204.1258](#).
- [53] PHENIX collaboration, A. Adare *et al.*, *Measurement of the relative yields of $\psi(2S)$ to $\psi(1S)$ mesons produced at forward and backward rapidity in $p + p$, $p + Al$, $p + Au$, and ${}^3He + Au$ collisions at $\sqrt{s_{NN}} = 200$ GeV*, Phys. Rev. **C95** (2017) 034904, [arXiv:1609.06550](#).
- [54] J.-P. Lansberg and H.-S. Shao, *Production of $J/\psi + \eta_c$ versus $J/\psi + J/\psi$ at the LHC: Importance of real α_s^5 corrections*, Phys. Rev. Lett. **111** (2013) 122001, [arXiv:1308.0474](#).
- [55] H.-S. Shao, *HELAC-Onia: An automatic matrix element generator for heavy quarkonium physics*, Comput. Phys. Commun. **184** (2013) 2562, [arXiv:1212.5293](#).
- [56] H.-S. Shao, *HELAC-Onia 2.0: An upgraded matrix-element and event generator for heavy quarkonium physics*, Comput. Phys. Commun. **198** (2016) 238, [arXiv:1507.03435](#).
- [57] Z.-G. He, B. A. Kniehl, M. A. Nefedov, and V. A. Saleev, *Double prompt J/ψ hadroproduction in the parton Reggeization approach with high-energy resummation*, Phys. Rev. Lett. **123** (2019) 162002, [arXiv:1906.08979](#).
- [58] A. V. Karpishkov, M. A. Nefedov, and V. A. Saleev, *$B\bar{B}$ angular correlations at the LHC in parton Reggeization approach merged with higher-order matrix elements*, Phys. Rev. **D96** (2017) 096019, [arXiv:1707.04068](#).
- [59] LHCb collaboration, R. Aaij *et al.*, *Measurement of J/ψ -pair production in pp collisions at $\sqrt{s} = 13$ TeV and study of gluon transverse-momentum dependent PDFs*, [arXiv:2311.14085](#), submitted to JHEP.

LHCb collaboration

R. Aaij³⁵, A.S.W. Abdelmotteleb⁵⁴, C. Abellan Beteta⁴⁸, F. Abudinén⁵⁴,
T. Ackernley⁵⁸, B. Adeva⁴⁴, M. Adinolfi⁵², P. Adlarson⁷⁸, H. Afsharnia¹¹,
C. Agapopoulou⁴⁶, C.A. Aidala⁷⁹, Z. Ajaltouni¹¹, S. Akar⁶³, K. Akiba³⁵,
P. Albicocco²⁵, J. Albrecht¹⁷, F. Alessio⁴⁶, M. Alexander⁵⁷, A. Alfonso Alberro⁴³,
Z. Aliouche⁶⁰, P. Alvarez Cartelle⁵³, R. Amalric¹⁵, S. Amato³, J.L. Amey⁵²,
Y. Amhis^{13,46}, L. An⁶, L. Anderlini²⁴, M. Andersson⁴⁸, A. Andreianov⁴¹,
P. Andreola⁴⁸, M. Andreotti²³, D. Andreou⁶⁶, A. Anelli^{28,n}, D. Ao⁷,
F. Archilli^{34,t}, S. Arguedas Cuendis⁹, A. Artamonov⁴¹, M. Artuso⁶⁶, E. Aslanides¹²,
M. Atzeni⁶², B. Audurier¹⁴, D. Bacher⁶¹, I. Bachiller Perea¹⁰, S. Bachmann¹⁹,
M. Bachmayer⁴⁷, J.J. Back⁵⁴, A. Bailly-reyre¹⁵, P. Baladron Rodriguez⁴⁴,
V. Balagura¹⁴, W. Baldini²³, J. Baptista de Souza Leite², M. Barbetti^{24,k}, I.
R. Barbosa⁶⁷, R.J. Barlow⁶⁰, S. Barsuk¹³, W. Barter⁵⁶, M. Bartolini⁵³,
F. Baryshnikov⁴¹, J.M. Basels¹⁶, G. Bassi^{32,q}, B. Batsukh⁵, A. Battig¹⁷,
A. Bay⁴⁷, A. Beck⁵⁴, M. Becker¹⁷, F. Bedeschi³², I.B. Bediaga², A. Beiter⁶⁶,
S. Belin⁴⁴, V. Bellee⁴⁸, K. Belous⁴¹, I. Belov²⁶, I. Belyaev⁴¹, G. Benane¹²,
G. Bencivenni²⁵, E. Ben-Haim¹⁵, A. Berezhnoy⁴¹, R. Bernet⁴⁸, S. Bernet Andres⁴²,
H.C. Bernstein⁶⁶, C. Bertella⁶⁰, A. Bertolin³⁰, C. Betancourt⁴⁸, F. Betti⁵⁶, J.
Bex⁵³, I.a. Bezshyiko⁴⁸, J. Bhom³⁸, M.S. Bieker¹⁷, N.V. Biesuz²³, P. Billoir¹⁵,
A. Biolchini³⁵, M. Birch⁵⁹, F.C.R. Bishop¹⁰, A. Bitadze⁶⁰, A. Bizzeti¹⁰,
M.P. Blago⁵³, T. Blake⁵⁴, F. Blanc⁴⁷, J.E. Blank¹⁷, S. Blusk⁶⁶, D. Bobulska⁵⁷,
V. Bocharnikov⁴¹, J.A. Boelhave¹⁷, O. Boente Garcia¹⁴, T. Boettcher⁶³, A.
Bohare⁵⁶, A. Boldyrev⁴¹, C.S. Bolognani⁷⁶, R. Bolzonella^{23,j}, N. Bondar⁴¹,
F. Borgato^{30,46}, S. Borghi⁶⁰, M. Borsato^{28,n}, J.T. Borsuk³⁸, S.A. Bouchiba⁴⁷,
T.J.V. Bowcock⁵⁸, A. Boyer⁴⁶, C. Bozzi²³, M.J. Bradley⁵⁹, S. Braun⁶⁴,
A. Brea Rodriguez⁴⁴, N. Breer¹⁷, J. Brodzicka³⁸, A. Brossa Gonzalo⁴⁴, J. Brown⁵⁸,
D. Brundu²⁹, A. Buonaura⁴⁸, L. Buonincontri³⁰, A.T. Burke⁶⁰, C. Burr⁴⁶,
A. Bursche⁶⁹, A. Butkevich⁴¹, J.S. Butter⁵³, J. Buytaert⁴⁶, W. Byczynski⁴⁶,
S. Cadeddu²⁹, H. Cai⁷¹, R. Calabrese^{23,j}, L. Calefice¹⁷, S. Cali²⁵, M. Calvi^{28,n},
M. Calvo Gomez⁴², J. Cambon Bouzas⁴⁴, P. Campana²⁵, D.H. Campora Perez⁷⁶,
A.F. Campoverde Quezada⁷, S. Capelli^{28,n}, L. Capriotti²³, A. Carbone^{22,h},
L. Carcedo Salgado⁴⁴, R. Cardinale^{26,l}, A. Cardini²⁹, P. Carniti^{28,n}, L. Carus¹⁹,
A. Casais Vidal⁶², R. Caspary¹⁹, G. Casse⁵⁸, J. Castro Godinez⁹, M. Cattaneo⁴⁶,
G. Cavallero²³, V. Cavallini^{23,j}, S. Celani⁴⁷, J. Cerasoli¹², D. Cervenkov⁶¹, S.
Cesare^{27,m}, A.J. Chadwick⁵⁸, I. Chahrour⁷⁹, M. Charles¹⁵, Ph. Charpentier⁴⁶,
C.A. Chavez Barajas⁵⁸, M. Chefdeville¹⁰, C. Chen¹², S. Chen⁵, A. Chernov³⁸,
S. Chernyshenko⁵⁰, V. Chobanova^{44,x}, S. Cholak⁴⁷, M. Chrzaszcz³⁸, A. Chubykin⁴¹,
V. Chulikov⁴¹, P. Ciambrone²⁵, M.F. Cicala⁵⁴, X. Cid Vidal⁴⁴, G. Ciezarek⁴⁶,
P. Cifra⁴⁶, P.E.L. Clarke⁵⁶, M. Clemencic⁴⁶, H.V. Cliff⁵³, J. Closier⁴⁶,
J.L. Cobbledick⁶⁰, C. Cocha Toapaxi¹⁹, V. Coco⁴⁶, J. Cogan¹², E. Cogneras¹¹,
L. Cojocariu⁴⁰, P. Collins⁴⁶, T. Colombo⁴⁶, A. Comerma-Montells⁴³, L. Congedo²¹,
A. Contu²⁹, N. Cooke⁵⁷, I. Corredoira⁴⁴, A. Correia¹⁵, G. Corti⁴⁶,
J.J. Cottee Meldrum⁵², B. Couturier⁴⁶, D.C. Craik⁴⁸, M. Cruz Torres^{2,f}, R. Currie⁵⁶,
C.L. Da Silva⁶⁵, S. Dadabaev⁴¹, L. Dai⁶⁸, X. Dai⁶, E. Dall'Occo¹⁷, J. Dalseno⁴⁴,
C. D'Ambrosio⁴⁶, J. Daniel¹¹, A. Danilina⁴¹, P. d'Argent²¹, A. Davidson⁵⁴,
J.E. Davies⁶⁰, A. Davis⁶⁰, O. De Aguiar Francisco⁶⁰, C. De Angelis^{29,i}, J. de Boer³⁵,
K. De Bruyn⁷⁵, S. De Capua⁶⁰, M. De Cian¹⁹, U. De Freitas Carneiro Da Graca^{2,b},
E. De Lucia²⁵, J.M. De Miranda², L. De Paula³, M. De Serio^{21,g}, D. De Simone⁴⁸,
P. De Simone²⁵, F. De Vellis¹⁷, J.A. de Vries⁷⁶, F. Debernardis^{21,g}, D. Decamp¹⁰,

E.J. Walton¹ , G. Wan⁶ , C. Wang¹⁹ , G. Wang⁸ , J. Wang⁶ , J. Wang⁵ , J. Wang⁴ ,
J. Wang⁷¹ , M. Wang²⁷ , N. W. Wang⁷ , R. Wang⁵² , X. Wang⁶⁹ , X. W. Wang⁵⁹ ,
Y. Wang⁸ , Z. Wang¹³ , Z. Wang⁴ , Z. Wang⁷ , J.A. Ward^{54,1} , N.K. Watson⁵¹ ,
D. Websdale⁵⁹ , Y. Wei⁶ , B.D.C. Westhenry⁵² , D.J. White⁶⁰ , M. Whitehead⁵⁷ ,
A.R. Wiederhold⁵⁴ , D. Wiedner¹⁷ , G. Wilkinson⁶¹ , M.K. Wilkinson⁶³ ,
M. Williams⁶² , M.R.J. Williams⁵⁶ , R. Williams⁵³ , F.F. Wilson⁵⁵ , W. Wislicki³⁹ ,
M. Witek³⁸ , L. Witola¹⁹ , C.P. Wong⁶⁵ , G. Wormser¹³ , S.A. Wotton⁵³ , H. Wu⁶⁶ ,
J. Wu⁸ , Y. Wu⁶ , K. Wyllie⁴⁶ , S. Xian⁶⁹ , Z. Xiang⁵ , Y. Xie⁸ , A. Xu³² , J. Xu⁷ ,
L. Xu⁴ , L. Xu⁴ , M. Xu⁵⁴ , Z. Xu¹¹ , Z. Xu⁷ , Z. Xu⁵ , D. Yang⁴ , S. Yang⁷ ,
X. Yang⁶ , Y. Yang^{26,l} , Z. Yang⁶ , Z. Yang⁶⁴ , V. Yeroshenko¹³ , H. Yeung⁶⁰ ,
H. Yin⁸ , C. Y. Yu⁶ , J. Yu⁶⁸ , X. Yuan⁵ , E. Zaffaroni⁴⁷ , M. Zavertyaev¹⁸ ,
M. Zdybal³⁸ , M. Zeng⁴ , C. Zhang⁶ , D. Zhang⁸ , J. Zhang⁷ , L. Zhang⁴ ,
S. Zhang⁶⁸ , S. Zhang⁶ , Y. Zhang⁶ , Y. Zhang⁶¹ , Y. Z. Zhang⁴ , Y. Zhao¹⁹ ,
A. Zharkova⁴¹ , A. Zhelezov¹⁹ , X. Z. Zheng⁴ , Y. Zheng⁷ , T. Zhou⁶ , X. Zhou⁸ ,
Y. Zhou⁷ , V. Zhovkovska¹³ , L. Z. Zhu⁷ , X. Zhu⁴ , X. Zhu⁸ , Z. Zhu⁷ ,
V. Zhukov^{16,41} , J. Zhuo⁴⁵ , Q. Zou^{5,7} , D. Zuliani³⁰ , G. Zunica⁶⁰ .

¹*School of Physics and Astronomy, Monash University, Melbourne, Australia*

²*Centro Brasileiro de Pesquisas Físicas (CBPF), Rio de Janeiro, Brazil*

³*Universidade Federal do Rio de Janeiro (UFRJ), Rio de Janeiro, Brazil*

⁴*Center for High Energy Physics, Tsinghua University, Beijing, China*

⁵*Institute Of High Energy Physics (IHEP), Beijing, China*

⁶*School of Physics State Key Laboratory of Nuclear Physics and Technology, Peking University, Beijing, China*

⁷*University of Chinese Academy of Sciences, Beijing, China*

⁸*Institute of Particle Physics, Central China Normal University, Wuhan, Hubei, China*

⁹*Consejo Nacional de Rectores (CONARE), San Jose, Costa Rica*

¹⁰*Université Savoie Mont Blanc, CNRS, IN2P3-LAPP, Annecy, France*

¹¹*Université Clermont Auvergne, CNRS/IN2P3, LPC, Clermont-Ferrand, France*

¹²*Aix Marseille Univ, CNRS/IN2P3, CPPM, Marseille, France*

¹³*Université Paris-Saclay, CNRS/IN2P3, IJCLab, Orsay, France*

¹⁴*Laboratoire Leprince-Ringuet, CNRS/IN2P3, Ecole Polytechnique, Institut Polytechnique de Paris, Palaiseau, France*

¹⁵*LPNHE, Sorbonne Université, Paris Diderot Sorbonne Paris Cité, CNRS/IN2P3, Paris, France*

¹⁶*I. Physikalisches Institut, RWTH Aachen University, Aachen, Germany*

¹⁷*Fakultät Physik, Technische Universität Dortmund, Dortmund, Germany*

¹⁸*Max-Planck-Institut für Kernphysik (MPIK), Heidelberg, Germany*

¹⁹*Physikalisches Institut, Ruprecht-Karls-Universität Heidelberg, Heidelberg, Germany*

²⁰*School of Physics, University College Dublin, Dublin, Ireland*

²¹*INFN Sezione di Bari, Bari, Italy*

²²*INFN Sezione di Bologna, Bologna, Italy*

²³*INFN Sezione di Ferrara, Ferrara, Italy*

²⁴*INFN Sezione di Firenze, Firenze, Italy*

²⁵*INFN Laboratori Nazionali di Frascati, Frascati, Italy*

²⁶*INFN Sezione di Genova, Genova, Italy*

²⁷*INFN Sezione di Milano, Milano, Italy*

²⁸*INFN Sezione di Milano-Bicocca, Milano, Italy*

²⁹*INFN Sezione di Cagliari, Monserrato, Italy*

³⁰*Università degli Studi di Padova, Università e INFN, Padova, Padova, Italy*

³¹*INFN Sezione di Perugia, Perugia, Italy*

³²*INFN Sezione di Pisa, Pisa, Italy*

³³*INFN Sezione di Roma La Sapienza, Roma, Italy*

³⁴*INFN Sezione di Roma Tor Vergata, Roma, Italy*

³⁵*Nikhef National Institute for Subatomic Physics, Amsterdam, Netherlands*

³⁶*Nikhef National Institute for Subatomic Physics and VU University Amsterdam, Amsterdam,*

Netherlands

- ³⁷ AGH - University of Science and Technology, Faculty of Physics and Applied Computer Science, Kraków, Poland
- ³⁸ Henryk Niewodniczanski Institute of Nuclear Physics Polish Academy of Sciences, Kraków, Poland
- ³⁹ National Center for Nuclear Research (NCBJ), Warsaw, Poland
- ⁴⁰ Horia Hulubei National Institute of Physics and Nuclear Engineering, Bucharest-Magurele, Romania
- ⁴¹ Affiliated with an institute covered by a cooperation agreement with CERN
- ⁴² DS4DS, La Salle, Universitat Ramon Llull, Barcelona, Spain
- ⁴³ ICCUB, Universitat de Barcelona, Barcelona, Spain
- ⁴⁴ Instituto Galego de Física de Altas Enerxías (IGFAE), Universidade de Santiago de Compostela, Santiago de Compostela, Spain
- ⁴⁵ Instituto de Física Corpuscular, Centro Mixto Universidad de Valencia - CSIC, Valencia, Spain
- ⁴⁶ European Organization for Nuclear Research (CERN), Geneva, Switzerland
- ⁴⁷ Institute of Physics, Ecole Polytechnique Fédérale de Lausanne (EPFL), Lausanne, Switzerland
- ⁴⁸ Physik-Institut, Universität Zürich, Zürich, Switzerland
- ⁴⁹ NSC Kharkiv Institute of Physics and Technology (NSC KIPT), Kharkiv, Ukraine
- ⁵⁰ Institute for Nuclear Research of the National Academy of Sciences (KINR), Kyiv, Ukraine
- ⁵¹ University of Birmingham, Birmingham, United Kingdom
- ⁵² H.H. Wills Physics Laboratory, University of Bristol, Bristol, United Kingdom
- ⁵³ Cavendish Laboratory, University of Cambridge, Cambridge, United Kingdom
- ⁵⁴ Department of Physics, University of Warwick, Coventry, United Kingdom
- ⁵⁵ STFC Rutherford Appleton Laboratory, Didcot, United Kingdom
- ⁵⁶ School of Physics and Astronomy, University of Edinburgh, Edinburgh, United Kingdom
- ⁵⁷ School of Physics and Astronomy, University of Glasgow, Glasgow, United Kingdom
- ⁵⁸ Oliver Lodge Laboratory, University of Liverpool, Liverpool, United Kingdom
- ⁵⁹ Imperial College London, London, United Kingdom
- ⁶⁰ Department of Physics and Astronomy, University of Manchester, Manchester, United Kingdom
- ⁶¹ Department of Physics, University of Oxford, Oxford, United Kingdom
- ⁶² Massachusetts Institute of Technology, Cambridge, MA, United States
- ⁶³ University of Cincinnati, Cincinnati, OH, United States
- ⁶⁴ University of Maryland, College Park, MD, United States
- ⁶⁵ Los Alamos National Laboratory (LANL), Los Alamos, NM, United States
- ⁶⁶ Syracuse University, Syracuse, NY, United States
- ⁶⁷ Pontifícia Universidade Católica do Rio de Janeiro (PUC-Rio), Rio de Janeiro, Brazil, associated to ³
- ⁶⁸ School of Physics and Electronics, Hunan University, Changsha City, China, associated to ⁸
- ⁶⁹ Guangdong Provincial Key Laboratory of Nuclear Science, Guangdong-Hong Kong Joint Laboratory of Quantum Matter, Institute of Quantum Matter, South China Normal University, Guangzhou, China, associated to ⁴
- ⁷⁰ Lanzhou University, Lanzhou, China, associated to ⁵
- ⁷¹ School of Physics and Technology, Wuhan University, Wuhan, China, associated to ⁴
- ⁷² Departamento de Física, Universidad Nacional de Colombia, Bogota, Colombia, associated to ¹⁵
- ⁷³ Universität Bonn - Helmholtz-Institut für Strahlen und Kernphysik, Bonn, Germany, associated to ¹⁹
- ⁷⁴ Eotvos Lorand University, Budapest, Hungary, associated to ⁴⁶
- ⁷⁵ Van Swinderen Institute, University of Groningen, Groningen, Netherlands, associated to ³⁵
- ⁷⁶ Universiteit Maastricht, Maastricht, Netherlands, associated to ³⁵
- ⁷⁷ Tadeusz Kosciuszko Cracow University of Technology, Cracow, Poland, associated to ³⁸
- ⁷⁸ Department of Physics and Astronomy, Uppsala University, Uppsala, Sweden, associated to ⁵⁷
- ⁷⁹ University of Michigan, Ann Arbor, MI, United States, associated to ⁶⁶
- ⁸⁰ Departement de Physique Nucleaire (SPhN), Gif-Sur-Yvette, France

^a Universidade de Brasília, Brasília, Brazil

^b Centro Federal de Educação Tecnológica Celso Suckow da Fonseca, Rio De Janeiro, Brazil

^c Hangzhou Institute for Advanced Study, UCAS, Hangzhou, China

^d LIP6, Sorbonne Université, Paris, France

^e Excellence Cluster ORIGINS, Munich, Germany

^f Universidad Nacional Autónoma de Honduras, Tegucigalpa, Honduras

^g Università di Bari, Bari, Italy

- ^h *Università di Bologna, Bologna, Italy*
ⁱ *Università di Cagliari, Cagliari, Italy*
^j *Università di Ferrara, Ferrara, Italy*
^k *Università di Firenze, Firenze, Italy*
^l *Università di Genova, Genova, Italy*
^m *Università degli Studi di Milano, Milano, Italy*
ⁿ *Università di Milano Bicocca, Milano, Italy*
^o *Università di Padova, Padova, Italy*
^p *Università di Perugia, Perugia, Italy*
^q *Scuola Normale Superiore, Pisa, Italy*
^r *Università di Pisa, Pisa, Italy*
^s *Università della Basilicata, Potenza, Italy*
^t *Università di Roma Tor Vergata, Roma, Italy*
^u *Università di Siena, Siena, Italy*
^v *Università di Urbino, Urbino, Italy*
^w *Universidad de Alcalá, Alcalá de Henares , Spain*
^x *Universidade da Coruña, Coruña, Spain*
^y *Department of Physics/Division of Particle Physics, Lund, Sweden*
[†] *Deceased*